UNIVERSITÀ DEGLI STUDI DI TORINO

Emplacement process of Ferrar Dolerite sheets at Allan Hills (South Victoria Land, Antarctica) inferred from magnetic fabric

Giulia Airoldi[1,*], James D. Muirhead[3], Elena Zanella[2,*], James D.L. White[1]

[1] *Geology, University of Otago, PO Box 56, 9054 Dunedin, New Zealand*

[2] *D.S.T., Università di Torino, via Valperga Caluso 35, 10125, Italy*

[3] *School of Environment, University of Auckland, Private Bag 92019, New Zealand*

* *ALP - Alpine Laboratory of Paleomagnetism, 12016 Peveragno, Italy*

ABSTRACT

We analyze ten representative intrusions from two sets of inclined diabase (Ferrar Dolerite) sheets exposed at Allan Hills (South Victoria Land, Antarctica), using petrographic and rock magnetic methods to determine microfabrics and infer magma flow directions. At least one diabase sample was collected at the margins of each intrusion. Magnetite and pyrrhotite contribute to magnetic fabrics of the samples. Thirty-six magnetic fabric directions, inferred from the mutual arrangement of either the magnetic lineation, or the magnetic foliation plane and local macroscopic flow indicators (e.g. horn-shaped apophyses and kinks) at the tips and margins of each intrusion reveal composite (i.e. both lateral and vertical) flow paths recorded along each intrusive segment.

Petrographic textures and multiple flow directions inferred at sheet-segment tips reveal that 'passive' injection of magma via hydrofracturing produced the local shallow LIP plumbing as a sill-dominated intrusive complex very close to, or intersecting the paleosurface. This contrasts with ‘classic’ arrays of either vertically or laterally injected blade-like dykes.

1. INTRODUCTION AND PREVIOUS WORK

Coinciding with the edge of the east Antarctic craton, the Ordovician proto-Transantarctic Mountains were the result of episodes of convergence and divergence that occurred during the early Paleozoic to Neoproterozoic Ross Orogeny. Products of the orogeny are metasedimentary rocks and granitoids. The orogeny was followed by over 100 million years of erosion, represented by the regional ‘Kukri erosion

surface' disconformity at the top of the basement rocks (Isaac *et al.*, 1996). More than 200 million years of almost undisturbed sedimentation (400 ~ 180 Ma) followed, taking place along the western flank of the Transantarctic Mountains and resulting in today's widespread but discontinuous outcrops of Beacon Supergroup sedimentary rocks, which have an overall estimated thickness of ~2.5 km (Barrett, 1981, Barrett, 1991). In the early Jurassic breakup of the Gondwana supercontinent began along its Pacific margin. Jurassic rifting between west and east Gondwana was related to impingement of the Bouvet plume below the supercontinent. Initial rifting coincided with the evolution of a triple junction located in the Weddell Sea rift basin (Elliot, 1999, Elliot and Fleming, 2000). The Ferrar large igneous province (LIP) formed along one of the arms of the triple junction, along the western edge of the Transantarctic Mountains. Products of the magmatic event are both extrusive (mafic volcaniclastic deposits grouped within the Mawson Formation, and lava flows, or Kirkpatrick basalts, cf. Fig. 1) and tholeiitic sills and inclined sheets. Such Antarctic diabase bodies are commonly referred to as "Ferrar Dolerite" intrusions (since Gunn and Warren, 1962), thus the term 'dolerite' will be used throughout this paper.

Fig. 1

The Ferrar province is defined by extensive sills, which range from less than one metre to hundreds of metres in thickness and are exposed for several hundreds of kilometres along the eastern flank of the Transantarctic Mountains (Elliot and Fleming, 2008, Leat, 2008 and references therein). In only a few cases these intrusions seem to have been connected to the surface by networks of interlinked inclined dolerite sheets (e.g. Coombs Hills, Guegan, 2006). Recent investigations of two localized arrays of intrusive sheets and transgressive sills at Allan Hills and Terra Cotta Mountain, South Victoria Land, reveal hydrofracture emplacement mechanics of the ~183 Ma Ferrar magmas at shallow crustal levels (Airoldi *et al.*, 2011, Muirhead *et al.*, 2011). Airoldi *et al*. (2011) show some evidence that magma may have once travelled close to the surface and injected inclined, and in places coalescing, magma-filled fractures. White *et al*. (2009) and Muirhead *et al*. (2011) demonstrate that sheet injection occurred locally as branch-outs from sill peripheries. This has important implications for the transportation of magma and the nature of eruptive activity at shallow levels in the Ferrar Large Igneous Province.

Similar findings are documented in other LIPs, such as the South African Karoo province (Polteau *et al.*, 2008) and the North Atlantic Igneous Province (Thomson, 2007). Recent experimental and numerical studies (e.g. Galland *et al.*, 2009, Menand, 2009) imply that sills are a key element in LIP intrusive systems. The concept of magma emplaced as 'peripheral sheets' classically implies uplift and buckling of strata during sill injection and subsequent exploitation of accompanying fractures by magma sheets (Johnson and Pollard, 1973). Although experimental, numerical, and field studies demonstrate that the intrusion of sills can be strongly influenced by the presence of weak layering (Mudge, 1968, Kavanagh *et al.*, 2006, Maccaferri *et al.*, 2011) more so than by any particular tectonic regime, the predominance of sill-fed sheets rather than steeply dipping dykes in the Ferrar LIP suggests that an extensional tectonic regime did not influence the overall geometry of the plumbing system at shallow depths (i.e. < 4 km depth; Muirhead *et al.*, 2011). These considerations, combined with evidence that some Ferrar sills breached the surface to feed eruptions, lead to the conclusion that the evolution of the province needs to be reconsidered in terms of its magma dynamics and mechanical interaction with the country rocks.

Although emplacement mechanisms of laccoliths and tabular intrusions are well studied (Menand 2009 and references therein), it is still poorly understood for many intrusive systems whether their geometry results from magma-driven fracturing during emplacement, or from "passive" occupation of either pre-existing structures or those opened tectonically during magma emplacement.

Magma flow modes (e.g. lateral vs vertical) can be reconstructed either from macroscopic flow-indicators preserved in places along the intrusions(e.g. Baer *et al.*, 2006), or by means of optical and/or magnetic petrofabric studies (Callot and Guichet, 2003, Bascou *et al.*, 2005). Anisotropy of magnetic susceptibility (AMS) is frequently measured to study the fabrics of mafic intrusions. In fact, magnetic fabric is known to reliably mimic microscopic petrofabrics (Tarling and Hrouda, 1993) and, consequently, AMS data can be used to systematically interpret directions of magma flow during emplacement. Magnetic studies substantiate the hypothesis of dominantly lateral feeding of magma from small localized chambers into large dyke swarms of LIPs, such as the Proterozoic McKenzie Dyke Swarm (Ernst and Baragar, 1992), or dykes exposed along the volcanic margin of east Greenland (Callot *et al.*, 2001). In a few cases, magnetic fabric data has been used to indicate the focus of magma injection (Ernst and Buchan, 1997, Craddock *et al.*, 2008).

The present paper presents petrophysical characteristics of Ferrar Dolerites intrusions exposed at Allan Hills, South Victoria Land. Allan Hills represents an inferred paleodepth of <1 km within the Ferrar plumbing system. Petrologic and magnetic fabric data obtained from forty-five segments on ten representative intrusions exposed in its central area, integrated with field relationships previously described by Airoldi *et al*. (2011) and with macroscopic flow-indicators, were studied to reconstruct the magma emplacement mechanisms and flow directions.

2. FIELD OBSERVATIONS AND PETROLOGY OF ALLAN HILLS FERRAR INTRUSIONS

Field relationships of intrusions

Ferrar Dolerite sills prevail in the western and eastern arms of the Allan Hills nunatak. Large sills crop out in the northern periphery of the northwest area, where blocks of country rock are locally engulfed within dolerite. Networks of thin sills and dolerite sheets predominate in the northeast arm of the nunatak. Here, there is no evidence for significant breakup of their roof of country rocks. Despite their rather complex geometries, such intrusions at Allan Hills define consistent NW-SE structural trends.

This is especially true in the nunatak's central area (map in Fig. 2), where Ferrar intrusions can be separated into two sets based on their crosscutting relations and geometric characteristics: the older A_I set forms an overall parallel swarm of both continuous and segmented, transgressive diabase bodies with NNW dominant strike. The younger set A_{II} is a weakly radial swarm of asymmetric dolerite segments (SE to SE dominant strike). Intrusions in this second set thicken towards their area of intersection, which is some 300 m west of Roscollyn Tor (Fig. 2).

Fig. 2

All intrusions have dip magnitudes between 0° and 90°, with most values < 60° and in directions opposite to that of host rock bedding (dipping shallowly to the east).

The Allan Hills dolerite sheets have lengths varying from 30 to 1500 m. Individual segments measured in the central sector of the nunatak vary from 300 to 7 m length. The intrusions have a relatively narrow range in thickness (20-600 cm, and over 70% are <2 m wide, cf. Airoldi *et al.*, 2011), and exhibit only local macroscopic textural variations along their length.

Macroscopic flow indicators and thermomechanical deformation

Field relationships at Allan Hills indicate a complex succession of multiple intrusions, and intersection and interaction of adjacent magma-filled cracks. Simple or complex, bifurcated terminations such as horns and small apophyses formed as a result of these processes, and now infill fractures of the damage zone between adjacent sheets. Simple sheet terminations and horns are either straight or curved, which is considered a result of the stability of the stress field around the propagating cracks (Weinberger *et al.*, 2000). The average trend and plunge of such features unequivocally constrain the local crack and magma flow *direction* of propagation (i.e. both lineation and sense of propagation, see Pollard *et al.*, 1975, Baer *et al.*, 2006).

Thermomechanical effects of intrusion are minimal: contact aureoles consist of a few cm thick rims of both chilled dolerite and baked and indurated sedimentary host rock. Hook-shaped irregularities of indurated sandstone, or ‘cusps’ (Pollard *et al*., 1975) are exposed at one location along sheet #03 (Fig. 2). Mineralized veins and slickensides, unmineralized *striae* and other surface-irregularities are locally carved in the indurated host rock walls of many intrusions. Disruption of the host sandstone is localized at some of the sheets' tips; macroscopically visible structureless volcaniclastic sediment (possibly liquefied during intrusion) around intrusions occurs locally in the Roscollyn Tor area.

In terms of both deformation and kinematics the features described above can be accounted for by several processes. Pollard *et al*. (1975) related 'cusps and grooves' to peripheral fingering of magma radially away from the centre of the Shonkin Sag laccolith (Montana, U.S.). Although the cusps observed at Allan Hills are very localized, it is plausible that lateral fingering of magma occurred along some of the most shallowly-dipping intrusions, such as #03.

Unmineralized and mineralized striae could be the result of either simple shear between the host rock and the intruding magma (Pollard *et al*., 1975), or relative displacement of country rock walls at either side of the intrusion during magma injection and solidification (e.g. Correa-Gomes *et al.*, 2001, Féménias *et al.*, 2004). However, in the absence of either other macroscopic features, or AMS data (see Knight and Walker, 1988, Correa-Gomes *et al*., 2001), their trend and plunge cannot be used to infer the absolute direction of the magmatic flow.

Kinematic information obtained from unmmineralized and mineralized striae along intrusions in the field area do not define a unique sense of motion around the intrusions. These differences, and the fact that these features are concordant with the local orientation of each dolerite sheet, suggest that the considered surface lineations are not related to post-Ferrar tectonics as inferred, for instance, by Craw and Findlay (1985) for the Taylor Glacier area, rather to syn-intrusive deformation. Whether such phenomenon is associated with relative movement between the host rock walls and rapidly solidifying intrusive magma, or with flow-related thermomechanical effects along such surfaces, cannot be conclusively demonstrated for all the observed striae. The striae represented in Fig. 2c are interpreted as 'marks' left by magma passing over a shallowly dipping wall before it transgresses laterally as a sill. Based on field evidence alone, magma flow is thus inferred to be 'upward' and oblique towards the transgression. At the nearby Coombs Hills nunatak, calcite veins were attributed to either syn-magmatic mineralizing fluids circulating at 180 Ma, or to post-Ferrar hydrothermalism at c. 100 Ma (Ballance and Watters, 2002). Calcite slickenfibres (see Fig. 14d in Airoldi *et al*., 2011) may be regarded as the result of 'dip-slip fault' behaviour, with the hanging wall of the intrusion moving relative to the footwall, but this conclusion cannot be supported on field relations alone.

As a consequence of the above considerations the orientations of horns and 'cusps and grooves' preserved on host rock walls were confidently used as local flow indicators. Conversely, the reliability of slickenfibres and veins as flow indicators was evaluated on a case-by-case basis, taking into account both field relationships and directional information derived from the petrophysical data (later in this paper).

Petrology of Ferrar dolerites

One fresh specimen per intrusion was sectioned to be analyzed petrographically. Nonweathered material was reduced to a fine powder to prepare fused glass beads and pressed powder disks for X-ray fluorescence (XRF) major and trace element analyses, to be run at the University of Otago, NZ.

All intrusions are compositionally and texturally similar, with small variations in crystal size depending on their thickness. Dolerites are porphyritic to glomeroporphyritic, with phenocrysts >4 mm in size common in A_I sheets e.g. in Fig. 3a-b. A_{II} intrusions have finer crystalline texture (3c). Mineralogy is dominated by plagioclase and less abundant clinopyroxene (pigeonite demonstrating green-brown pleochroism, in Fig. 3b, and augite, orange-brown coloured, top right corner of 3c). A few of the largest clinopyroxene phenocrysts subophitically enclose prisms of plagioclase (3a).

Fig. 3

Plagioclase crystals demonstrate either normal zoning under polarized light or appear hollow and infilled with dark-brown to golden cryptocrystalline material ('hopper' texture, 3b). Clinopyroxene crystals can be both zoned and unzoned. Groundmass is commonly formed by randomly oriented microlites of idiomorphic, tabular and acicular plagioclase crystals (500 - 100 μm in size); acicular pyroxene crystals are intergranular. Clusters of radiating blades of plagioclase occur in thin sections of dolerite with finer crystal size (average ~200 μm, 3c). The cryptocrystalline glass constitutes an intersertal matrix containing dispersed granules of both pyrrhotite and magnetite, and locally stained by iron oxide alteration. Where abundant, the quenched glass groundmass is observed to be altered to optically isotropic palagonite and clay minerals (3d).

No clear compositional distinction can be made between the intrusive sets on the base of the normalized whole rock major elements and trace element data of twelve fresh representative samples (see Airoldi, 2011).

Geochemically all the investigated samples are considered basaltic andesites and andesites of intermediate composition (Table 1). The linear trends on variation diagrams in Fig. 4 are expected for typical differentiation series by fractional crystallization controlled by precipitation of plagioclase and

clinopyroxene. The same linear relationship is reflected in the Cr-Mg# variation, with Cr a trace element highly compatible with clinopyroxene, and further demonstrated by the Sr vs. Rb trend.

Table 1

Fig. 4

3. SAMPLING AND ANALYTICAL TECHNIQUE

Seven A_I intrusive sheets and three A_{II} segmented dykes were selected for rock magnetic, petrographic and geochemical analyses on the grounds of their good exposure and geometric characteristics (Fig. 2). Intrusions are either long and continuous or variably segmented, and in places multiply intruded. Locally, they exhibit kinematic indicators such as horn-apophyses and sidesteps along their selvages and/or surface lineations on their host rock walls.

Block samples of ~10 x 10 x 15 cm were oriented with both solar and magnetic compasses and a clinometer. A total of 84 samples were collected close to the intrusion margins, where both flow direction and sense of propagation may be preserved as mineral arrays and imbrications upon rapid cooling of magma (Knight and Walker, 1988). Sampling across dykes and in interiors used by other authors (e.g. Féménias *et al.*, 2004) was not possible due to the geometrical features and size of Allan Hills sheets.
At Allan Hills, collection of one sample at each margin was accomplished at a few locations along intrusions #04-07 and #14, because only one dyke margin is commonly exposed (Fig. 2). The mutual arrangement of the samples along each intrusive segment varied according to the length and thickness of each segment, and the alteration and jointing of the dolerite. Ideally, two samples would be collected at the tips of the segments, where flow indicators recurred, and one from the thickest, central portion of the segment. All samples were subsequently prepared for analysis in the Otago Palaeomagnetic Research Facility (OPRF) of the Geology Department of the University of Otago, NZ.

Between 5 and 15 core-specimens for rock magnetism analyses were obtained from each of the oriented block samples, for a total of 653 specimens. Magnetic susceptibility and its anisotropy were measured at OPRF using an AGICO MFK1-A Kappabridge. Susceptibility versus temperature analyses were run for selected specimens (at least one per intrusion) using a CS-3 furnace. Isothermal remanent

magnetization was studied at the ALP laboratory. IRM acquisition and thermal demagnetization, and backfield curves were measured for selected specimens (at least one per sheet) according to the Lowrie (1990, 1997) method and using a JR-6 spinner magnetometer. IRM anisotropy was measured for at least 5 specimens per sheet. Each specimen was first tumbling demagnetized at 60 mT peak-field, given an IRM applying a 20 mT direct field, and then measured. The procedure was repeated in six different orientations of the specimen relative to the field (after Potter and Stephenson, 1988, Potter, 2004).

4. FERRAR DOLERITE PETROPHYSICAL PROPERTIES AND MAGNETIC CARRIERS

The low-field magnetic susceptibility and coercivity spectra of at least one dolerite specimen per intrusion were analyzed both in isothermal conditions and upon thermal treatment. Dolerite specimens of both intrusive sets reveal a wide range of mean magnetic susceptibilities (415 - 30428 μSI, with an average k_m value of 5620 μSI for the entire dataset) but show, otherwise, comparable thermomagnetic and isothermal behaviours, Curie temperatures and values of the remanence coercive force. The degree of anisotropy P_J is normally below 1%, but may reach values as high as 1.045. For simplicity of analysis, the Allan Hills specimens are subdivided into three susceptibility groups, where 'low-', 'intermediate-' and 'high-susceptibility' specimens are characterized, respectively, by K_m values in the orders of 10^{-4}, 10^{-3} and 10^{-2} SI (Fig. 5).

Fig. 5

Ferrar Dolerite $k_b(T)$ curves of representative specimens (top row in Fig. 6) are irreversible. This phenomenon is commonly related to occurrence of alteration i.e. transformation/production of ferromagnetic oxides upon heating (Henry, 2007). Almost reversible, however, is the thermomagnetic behaviour observed in intermediate-susceptibility specimens, where the $k_b(T)$ heating path frequently shows a Hopkinson peak between 300° and 460° C (6b). The occurrence of such Hopkinson peaks, and shape of a few thermomagnetic curves, are features normally related to assemblages of both SD and MD grains in the rock fabric, where the anomalous peaks reveal remanence unblocked at higher

temperatures due to domain-wall freedom, and therefore indicate predominance of MD magnetite among the rock magnetic carriers (Potter and Stephenson, 1988, Rochette *et al.*, 1999).

Magnetic minerals with both soft (B_{CR}<0.5 T) and medium (0.5<B_{CR}<1 T) remanence coercivity share most of the total magnetization of the dolerite (J/T curves in Fig. 6). Over ~60% of the magnetization of low- and high-susceptibility specimens is due to low coercivity magnetic fractions; medium remanence coercivity phases contribute ~35% or less. In intermediate-susceptibility specimens similar quantities of soft and medium remanence coercivity fractions contribute ≥80% of the rock magnetization (example 6b). Less than 20% (<10% in the intermediate susceptibility specimens) of the total magnetization is carried by a 'hard' magnetic fraction (B_{CR}>1 T). All remanence coercivity fractions show a steeper decay of magnetization approaching 200°C, which translates into steepening of the remanent magnetization curves for soft and medium fractions, and complete erasure of hard coercivity phases between 200° and 300°C. K_b paths are relatively regular during the progressive thermal demagnetization of the Lowrie analyses, and show that thermomagnetic behaviours were not controlled by mineralogic transformations.

Both thermomagnetic methods allow identification of Curie temperatures between 550° and 650° C, but more frequently above 600° C.

IRM saturates at values of applied field (B_S) around 300 mT. A coercive remanence field (B_{CR}) of normally 30-40 mT, and in a few instances around 70-80 mT (Fig. 6a), cancels the magnetization of the rock.

Fig. 6

The wide distribution of magnetic susceptibilities observed, as well as the evidence for both 'high' (70-80 mT) and 'soft' (B_{CR}=30 mT) magnetic remanence coercivity fractions, can indicate the presence of either different ferromagnetic minerals and/or variable grain-size of the magnetic carrier(s), or both. The magnetic susceptibility values are, however, typical of many igneous rocks where Fe-Ti oxides are distributed inhomogeneously (Tarling and Hrouda, 1993).

Curie temperatures and B_S and B_{CR} values are characteristic of at least two principal magnetic phases in the Allan Hills Ferrar Dolerites: Curie points up to 575° C and low remanence coercivity values are typical of magnetite, whereas similar B_{CR} values corresponding to higher Curie temperatures (Tc=590°-675° C)

may either indicate maghemite and/or magnetite oxidized to haematite (Borradaile, 1988, deBoer and Dekkers, 1996).

The presence of magnetite (or maghemite) and pyrrhotite justifies the Curie temperatures identified with thermomagnetic measurements. Coercivity and IRM properties are also consistent with the presence of such minerals within the dolerites' petrofabric. Specifically, the common inflection of the remanent magnetization curves of different coercivity fractions around 100 - 300° C is typical reflection of the breakdown of pyrrhotite.

5. MAGNETIC FABRIC

Magnetic anisotropy of rocks

The anisotropy of magnetic susceptibility (AMS) in rocks is modelled as an ellipsoid with mutually orthogonal axes $k_1>k_2>k_3$ (respectively, maximum, intermediate and minimum axes), graphically plotted as lineations on equal area stereographic projections. AMS is commonly studied to investigate the overall magnetic fabric of a rock, whereas anisotropy of remanence magnetization (ARM) analyses are performed only occasionally (i.e. when specific investigation of the type of magnetic domain is needed) (Potter and Stephenson, 1988). Mean magnetic susceptibility (k_m), magnetic lineation (L) and foliation (F), anisotropy degree (P or P_J, corrected anisotropy degree) and shape parameter (T) are the anisotropy parameters defined for any magnetic fabric ellipsoid. They are mathematically expressed as reported by Tarling and Hrouda (1993, Table 1.1, p. 18). The anisotropy degree defines the absolute anisotropy of a rock specimen. L, F and T concur to define the geometry of the AMS ellipsoid. Prolate fabric ellipsoids are elongate (L>F) and characterized by $-1 \geq T > 0$, whereas oblate ellipsoids are flattened (F>L) and characterized by $0 > T \geq 1$. In the directional analysis of AMS fabrics, magnetic lineation and foliation correspond respectively to the maximum susceptibility axis direction k_1, and to the plane perpendicular to k_3 and defined by k_1 and k_2. Analogous considerations can be made for the ARM.

Magnetic fabric of igneous dykes and sills

AMS fabrics of igneous intrusions result from the hydrodynamic alignment of crystals during magma flow (e.g. Knight and Walker, 1988). Ferromagnetic minerals such as magnetite, titanomagnetite and other Fe-

Ti oxides crystallize late i.e. after the flow ceased, in textural gaps and/or along the edges of preformed crystals, thus mimicking the alignment of the earlier-crystallized, non-ferromagnetic minerals.

Ideally, dykes present a magnetic fabric characteristically prolate, with magnetic lineation (k_1, or i_1 in the case of anisotropy of isothermal remanence magnetization, or AIRM fabrics) parallel to the plane of the intrusion and indicating the flow direction (Tarling and Hrouda, 1993, Rochette *et al*., 1999). The magnetic foliation plane and the dyke plane can either be co-aligned, or imbricated with respect to it. The imbrication angle is characteristically ≤30° ('normal fabrics' - Knight and Walker, 1988, Tauxe *et al.*, 1998), but can be up to 45° ('intermediate' fabrics, e.g. Dragoni *et al.*, 1997). Intermediate fabrics are commonly related to either mixing, or alternating magnetic behaviour, of AMS sources with different properties, such as prolate and oblate magnetic particles within the rock, and are reflected by the exchange of the intermediate and minimum axes of the fabric ellipsoid (e.g. Knight and Walker, 1988, Raposo and Ernesto, 1995, Ferré, 2002, Herrero-Bervera *et al.*, 2002, Cañón-Tapia and Herrero-Bervera, 2009 and references therein).

Finally, 'inverse' fabrics are 'anomalous' fabrics characterized by minimum susceptibility axis aligned within the dyke plane, and the magnetic foliation perpendicular to the dyke; such fabrics are relatively uncommon and related to the presence of single-domain magnetic grains within the rock fabric (e.g. Rochette *et al.*, 1999).

Allan Hills magnetic fabric data

Over 60% of the Allan Hills fabric data can be interpreted as either 'normal' or 'intermediate' magnetic fabrics. Normal fabrics are about 20% of the dataset. For dykes sampled along both their margins, the resulting magnetic fabric is also 'scissored' (Fig. 7). Such fabric is formed by two distinct k_1 clusters, grouped at either side of the sheet intrusion, which converge along the trace of the dyke plane and thus identify the mean magnetic lineation and the absolute flow direction (Knight and Walker, 1988, Correa-Gomes *et al*., 2001). In the example given in Fig. 7, data clusters come from both AMS and AIRM measurements (later in text).

Fig. 7

Intermediate magnetic fabrics are over 40% of the dataset: they are here subdivided into three classes, each one characterized by a specific arrangement of the fabric ellipsoid axes:

I_1, commonly prolate, with the magnetic lineation lying on, or within 45° from the dyke plane and other two axes of the fabric ellipsoid dispersed on a girdle (top right corner in Fig. 8).

I_2, i.e. a magnetic fabric with both maximum and minimum axes of the magnetic fabric ellipsoid aligned in the plane of the intrusion and magnetic foliation plane perpendicular to it (Fig. 8).

I_3, nearly *normal* planar fabric, where the magnetic lineation is anomalous and the intermediate susceptibility/remanence axis lies closest to the plane of the dyke. Dyke and magnetic foliation planes are subparallel, as in normal fabrics, but imbrication (or intersection, bottom right stereoplot in Fig. 8) angles are >30°.

Fig. 8

Finally, 26% of the data are either inverse fabrics or nearly isotropic AMS results and were disregarded from the interpretation (i.e. with low values in tests of anisotropy and/or corrected anisotropy degree PJ <1.005, cf. Jelinek, 1978). Only in a few cases, where the magnetic fabric is characterized by $P_J \leq 1.004$ but the clusters of magnetic fabric axes show little dispersion, data were still considered for directional interpretation.

AIRM results

The anisotropy of isothermal remanent magnetization was measured on dolerite specimens from eleven sites with either inverse AMS fabric or fabric characterized by chaotic clusters and low anisotropy parameters (about 30% of the overall dataset). Three normal and six intermediate resulting AIRM fabric types provide reliable directional information. In the example given in Figure 8b, for instance, a ‘normal’ arrangement of the AIRM axes underlies a reverse AMS fabric and yields a steeply plunging westward

flow direction, consistent with the orientation and AMS measurements from other sites of intrusion #11. Two inverse AIRM fabrics were discarded.

AMS ellipticity or fabric do not seem to correspond to a specific AIRM fabric type (diagram 8c); SD particles are not strikingly highlighted by inverse correlation of AMS and AIRM normalized vectors (Potter and Stephenson, 1988, cf. diagram 8d).

From the above considerations, magma flow directions of Allan Hills dolerite sheets can be reliably inferred from normal and intermediate fabrics. In oblate intermediate fabrics, all mean susceptibility/remanence axes may not lie directly in the flow plane, but the intersection between dyke plane and magnetic foliation plane is a good proxy of the magma flow direction. Where the intermediate susceptibility/remanence axis is within 30° of the plane of the intrusion (all four I_3 fabrics and one normal fabric with imbrication angle <30°, cf. Tables 2.a,b) it may be used as a flow indicator (lineation, see Herrero-Bervera *et al.*, 2001 and references therein) that coincides with the dyke/magnetic foliation planes intersection.

6. INTEGRATION OF RESULTS

Previous field reconstructions by Airoldi *et al*. (2011) and Muirhead *et al*. (2011) (1) locate the overall intrusive system at very shallow depth, as also inferred for other nearby locations (Shapeless Mountain: Korsch, 1984, Coombs Hills: White *et al.*, 2009), and (2) relate the two intrusion sets to a hidden 'sill' source. Additionally, Airoldi *et al*. (2011) infer a localized point of injection for the A_{II} set intrusions. From a structural point of view, A_I and A_{II} sheets, coupled with the Ferrar sills exposed throughout the province, are unusual in an extensional rift-system scenario such as that inferred for the Ferrar LIP and its south-african co-respective, the Karoo LIP (Muirhead *et al*., 2011 and references therein). Field and petrophysical data reported here are integrated to clarify these points.

Petrological constraints

No significant petrological differences distinguish dykes of the A_I and A_{II} sets, which have similar bulk compositions and geochemical signatures typical of Ferrar Dolerite rocks (see Leat, 2008, Ross *et al.*, 2008). Rock textures are characteristic of magma solidified at shallow crustal depths (see Rollinson, 1993, Winter, 2001). Evidence of rapid cooling is provided by chilled dolerite margins and minimal thermomechanical deformation of the host rock around the intrusions.

Plagioclase and clinopyroxene (pigeonite and augite) are the principal mineral phases; intergranular clinopyroxene crystals, ferromagnetic granules (pyrrhotite and magnetite) and clay minerals are enclosed in both main phases and in places within the glassy groundmass (cf. Airoldi, 2011). The presence of ferromagnetic pyrrhotite and magnetite is also demonstrated by rock magnetic properties, and validates the interpretation of 'normal' and 'intermediate' magnetic fabrics on the basis of the magnetic lineation direction k_1 and magnetic foliation plane. Intermediate fabrics may be either a result of co-existing normal and inverse particles (MD and SD magnetic grains), or prolate and oblate particles (magnetites and pyrrhotites, respectively). The occurrence of SD particles, however, is not conclusively demonstrated in specimens with inverse fabric and tested with AIRM technique.

Magma flow close to the surface

Magnetic fabrics of Allan Hills dykes are related to dyke orientations and matched with kinematic information on dyke propagation provided by both the arrangement of segments (e.g. *en echelon*) and lineations obtained from horns at segment tips and striations on their walls. Magma flow directions are defined by the orientation of either the magnetic lineation k_1, or the intersection between the magnetic foliation and dyke plane. Tables 2.a,b summarize the average AMS and/or AIRM parameters and flow directions from 36 dyke sections obtained from the Allan Hills dykes; 'sections' comprise magnetic fabric of all specimens collected from the same sheet segment. Where magnetic fabrics of specimens from distinct but adjacent and co-aligned segments are consistent with one another, they are also grouped into a single dyke section. Despite a slight prevalence of 'anomalous' intermediate magnetic fabrics, no particular fabric type characterizes any specific intrusion.

Table 2a

Table 2b

A distinct mode of magma propagation (lateral vs. vertical) is difficult to establish for each intrusive set, because vertical and lateral flow are both recorded along sheet segments belonging to larger intrusions. In general, lateral flow in the N-S (or NW-SE) direction is shared by more-continuous and regular dykes of both the A_I and A_{II} sets, whereas heterogeneous and generally steeper magma flow paths are defined by magnetic fabrics of highly segmented intrusions (Fig. 9). Horizontal flow is recorded at the tips of a few dyke segments.

Fig. 9

Overall, magnetic fabrics define flow paths that are strongly conditioned by the geometry of the host crack and/or local stress conditions. This is exemplified by the westernmost segment tip section #01-2t (Fig. 10). Here, the shape of the tip is complicated by two horns formed only a few tens of cm from where dyke

propagation was arrested. AMS results show an anomalous inverse fabric, whereas the AIRM fabric is intermediate with a subvertical flow lineation. This contrast could represent a composite microscopic fabric, which resulted when magma became trapped in a highly strained and fractured area. Consequently, magma began infilling fractures of the damage zone, with resulting, distinct flow-paths recorded by magnetic properties within localized areas.

Fig. 10

The rock fabric evidence given here may confirm both the model first proposed by Dragoni *et al*. (1997) for the Prince Albert Mountains sills (and thus the hypothesis of a cyclical evolution of magnetic fabric, as in Cañón-Tapia and Herrero-Bervera, 2009), and the inference of complex flow within the magma-filled cracks. Both conclusions may be interpreted in terms of either complex magnetic mineralogy, as seems reasonable from evidence in this paper, or of 'turbulent' flow during emplacement. Turbulent flow is considered unlikely, however, because Ferrar magmas would not have had a sufficiently high Reynolds number during intrusion in the thin tension fractures exposed at Allan Hills (see Fialko and Rubin, 1999). As an alternative, the hypothesis of crack-led injection of rapidly solidifying magma into highly strained areas (narrow and segmented tension cracks with greatest geometrical complexity at their tips) is preferable. At the large scale, addition of magma into the intrusive magma-filling body stresses the surrounding rock and causes the fracture to propagate. The magma just behind the tip is not the main driver in pushing the crack forward, and instead experiences an underpressured zone, into which it is drawn, as the crack opens. Fracture propagation may be uneven and/or intermittent, and thus cause locally complex flow paths as the magma flows to the tip.

In this sense, ‘passive’, crack-led magma propagation can be regarded as a style of magma injection that yields irregular flow paths without implying turbulent flow. Specifically for the Allan Hills example, 'simple' cooling of magma emplaced at shallow depths by this process accounts for both field and magnetic evidence.

Regional volcanological constraints

Data from this study reveal shallow intrusion dynamics over length scales no greater than 3 km. Many studies investigating regional magma flow paths sparsely sample dyke swarms over distances of 100s to 1000s of km. Sheet swarms in the Ferrar Dolerite, however, have not been traced over distances > 10 km. These short length scales suggest that shallow-level sheet arrays in Ferrar Dolerite were not responsible for the mass lateral transport of magma through the province, in agreement with recent studies revealing that exposed Ferrar sheets represent localized distribution networks within the overall magma system (White *et al*., 2009, Airoldi *et al*., 2011, Muirhead *et al*., 2011).

The magnetic fabric data do not conclusively point to a definite source(s) for the Allan Hills dykes. As for the A_{II} intrusions, their magnetically inferred flow directions are somewhat chaotic and the greatest evidence about a localized point of injection lies in the geometry of the intrusion array itself; magma flow appears to have been mostly vertical at the core of individual segments, and lateral at their tips. Similarly, magnetic lineations indicate both lateral and vertical flow in the continuous segments and transgressive A_I intrusions, with a slight predominance of lateral flow-paths, but do not indicate a source. Based on solely on their sub-parallel alignment, these dolerite sheets could be considered part of a regional dyke swarm developed in the (inferred) early-Jurassic extensional boundary of east Gondwana. Their formation as part of a regional dyke swarm has, however, been dismissed by previous authors, who considered: (1) the shallowly dipping, transgressive geometry of the described intrusions; (2) that the sheets exhibit remarkably short lengths and are not observed in neighbouring nunataks; (3) the lack of observable steeply dipping, parallel dyke swarms throughout the entire Ferrar LIP; (4) the inferred environment of emplacement (White *et al*., 2009, Muirhead *et al*., 2011), which is not conducive to forming long, sub-parallel dyke sets. Instead, magma-filled cracks of varying orientations seem to have formed as a consequence of a predominantly brittle response of the host rocks to magma injection (White *et al*., 2009, Airoldi *et al*., 2011). Additionally, parallel dykes should exhibit lateral flow directions consistently pointing to a major area of injection (e.g. from distal parts of giant dyke swarms, Ernst and Baragar, 1992, Callot *et al*., 2001), or vertical flow paths indicating ascent of magma through dykes or fissures in rift-systems

(cf. Ernst and Buchan, 1997, Callot and Geoffroy, 2004, Craddock *et al.*, 2008), but this is not the case at Allan Hills.

One explanation for the complex relationships between intrusion geometry and complex magma flow directions may be that magma was 'passively' fed into clusters of inclined fractures resulting from multiple sill inflation events. This hypothesis is in part supported by Airoldi *et al*. (2011) and Muirhead *et al*. (2011) who interpret the shallow dips and sub-parallel alignment of Allan Hills intrusions to reflect stresses associated with the emplacement of an underlying sill. It is additionally feasible that a second sill intersected this zone, and exploited the same discontinuities formed during contemporaneous doming of the underlying sill, which controlled the overall geometry of the resulting swarm. Given that contemporaneous emplacement of sills at multiple stratigraphic levels is expected in sill complexes (see Muirhead *et al*., 2011, and references therein) this hypothesis merits further investigation, and could be addressed through AMS studies of sheet swarms in South Victoria Land in areas such as Coombs Hills, Mt Gran, and Terra Cotta Mountain. Nonetheless, the magnetic fabric directions presented in this paper provide sufficient evidence that the intrusions at Allan Hills represent a distinctly magmatic style of crustal deformation. Although it is unlikely that these intrusions form a swarm responsible for distribution of proportionally large volumes of magma through the province, the swarm may yet indirectly reflect the regional magma flow at depth or in the Beacon Supergroup in the South Victoria Land region.

Other Ferrar analogues to the Allan Hills intrusive network

Large Ferrar Dolerite sills make up most of the Convoy Ranges and greatest proportion of the northern highlands at Coombs Hills (< 5 km south of Allan Hills, Fig. 3 in Ross *et al*., 2008). Ross *et al*. (2008) and White *et al*. (2009) related the hydromagmatic activity at Coombs Hills to interaction between shallow-seated magma and groundwater, prior to the emplacement of Kirkpatrick flood lavas in this region, based on the evidence provided by intra-vent primary volcaniclastic deposits cut by large clastic dykes, but the dolerite intrusions exposed here were otherwise poorly studied.

A > 200 m thick sill is well exposed along the northern top margin of the nunatak; it shows horizontal layering and intra-sill cooling margins related to multiple intrusions. Large rafts of both Beacon sediments and Mawson rocks 'float' within the dolerite and are intruded by dolerite sheets of all orientations (White

and Garland, 2007). Specifically, Beacon rafts are pervasively fractured and/or ductilely bent, with locally mingled magma and sediment forming fluidal peperite structures. Measurements of preserved bedding planes show that the rafts were tilted < 30° (Garland, 2006).

Inclined dolerite sheets (0.5 – 2 m thick) and rare sills (< 2 m thick) crop out both within in-place stratified Victoria Group sediments and unbedded volcaniclastic Mawson deposits, in a ~2 km^2 area north-west of Mount Brooke (Fig. 9, and see Guegan, 2006). Although heterogeneously distributed and highly segmented, subvertical dykes and inclined sheets define two distinct N-S and NW-SE oriented sets (Guegan, 2006). Dolerite bodies propagated across Beacon rocks have either en echelon geometry, with a dextral sense of displacement, or form irregular braided networks. Individual intrusion segments exhibit stepped and swirly geometries; crosscuts are localized and do not permit assessment of specific chronologic relationships among dykes. Joints in the country rock replicate the geometry of the intrusions, forming two intersecting arrays of N-S and NW-SE fractures, and in places those dip shallowly to the west (~40°). No other sign of either brittle or ductile deformation subsequent to intrusion is documented.

The above synthesis of intrusive field relationships leads us to conclude that the Coombs Hills sill, progressively thickened below the Jurassic paleosurface, breached through a 'weak' blanket of Beacon and Mawson sedimentary rocks and eventually intersected the surface. It cannot be said whether this same sill, or a different one, fed the intrusive network at Allan Hills, but factors such as the geometrical similarity between sheet intrusions, and the structural evidence of the evolution of large sills very close to (or intersecting) the Jurassic paleosurface (White *et al.*, 2009, Airoldi *et al.*, 2011) leave such an inference as a possibility.

A way to further investigate this hypothesis would be to test it with AMS analyses, i.e. by comparing flow directions of both the Coombs Hills sill and some of the largest sills exposed at Allan Hills, and those of the above exposed sheet and dyke networks.

7. CONCLUSIONS

A_I and A_{II} Ferrar Dolerite intrusions exposed at Allan Hills and thoroughly described in a recent study are studied with petrologic and rock magnetic methods. Ferromagnetic magnetite and pyrrhotite contribute to the magnetic fabric of the intrusions. 'Normal' and 'intermediate' relationships between each intrusion's plane and/or local field indicators and magnetic fabric allow the distinction of both lateral and vertical magma flow directions. Composite magma flow-modes can be described at the scale of single sheet segments, depending on their geometry. Such complex flow paths recorded in Allan Hills' sheets diverge from classical depictions of magma flow in both localized sheet arrays and regional dyke swarms. In the absence of conclusive evidence for localized feeders, magma represented by the first-cooled sheet margins is considered to have been drawn into advancing crack tips, which are highly strained areas (i.e. narrow and geometrically chaotic hydrofractures) driven ahead of growing sheets formed above (a) shallow-seated magmatic source(s), one of which may be preserved at Coombs Hills.

References

Airoldi, G.M., 2011. Magma injection dynamics in the shallow Ferrar LIP (South Victoria Land, Antarctica). Doctor of Phylosophy PhD, University of Otago, Dunedin.

Airoldi, G.M., Muirhead, J.D., White, J.D.L. & Rowland, J., 2011. Emplacement of magma at shallow depth: insights from field relationships at Allan Hills (South Victoria Land, East Antarctica). *Antarctic Science,* 23**,** 281-296, doi: 10.1017/S0954102011000095.

Baer, G., Aharon, L., Heimann, A., Shaliv, G. & Agnon, A., 2006. The Nahal Tavor vent: Iterplay of Miocene tectonics, dikes, and volcanism in the Lower Galilee, Israel, *Israelian Journal of Earth Science,* 55**,** 1-16, doi.

Ballance, P. & Watters, W.A., 2002. Hydrothermal alteration, contact metamorphism and authigenesis in Ferrar Supergroup and Beacon Supergroup rocks, Carapace Nunatak, Allan Hills and Coombs Hills, Victoria Land, Antarctica, *New Zealand Journal of Geology and Geophysics,* 45**,** 71-84, doi.

Barrett, P.J., 1981. History of the Ross Sea region during the deposition of the Beacon Supergroup 400-180 million years ago, *Journal of the Royal Society of New Zealand,* 11**,** 447-458, doi.

Barrett, P.J., 1991. The Devonian to Jurassic Beacon Supergroup of the Transantarctic Mountains and correlatives in other parts of Antarctica, *Oxford Monographs on Geology and Geophysics,* 17**,** 120-152, doi.

Bascou, J., Camps, P. & Marie Dautria, J., 2005. Magnetic versus crystallographic fabrics in a basaltic lava flow, *Journal of Volcanology and Geothermal Research,* 145**,** 119-135, doi.

Borradaile, G.J., 1988. Magnetic susceptibility, petrofabrics and strain, *Tectonophysics,* 156**,** 1-20, doi.

Callot, J.P. & Geoffroy, L., 2004. Magma flow in the East Greenland dyke swarm inferred from study of AMS: growth of a volcanic margin., *Geology Journal International,* 159**,** 816-830, doi.

Callot, J.P., Geoffroy, L., Aubourg, C., Pozzi, J.P. & Mege, D., 2001. Magma flow directions of shallow dykes from the East Greenland volcanic margin inferred from magnetic fabric studies, *Tectonophysics,* 335**,** 313-329, doi.

Callot, J.P. & Guichet, X., 2003. Rock texture and magnetic lineation in dykes; a simple analytical model, *Tectonophysics,* 366**,** 207-222, doi.

Cañón-Tapia, E. & Herrero-Bervera, E., 2009. Sampling strategies and the anisotropy of magnetic susceptibility of dykes. *in Tectonophysics*, pp. 3-17Elsevier B.V.

Correa-Gomes, L.C., Souza Filho, C.R., Martins, C.J.F.N. & Oliveira, E.P., 2001. Development of symmetrical and asymmetrical fabrics in sheet-like igneous bodies: the role of magma flow and wall-rock displacements in theoretical and natural cases, *Journal of Structural Geology,* 23**,** 1415-1428, doi.

Craddock, J.P., Kennedy, B.C., Cook, A.L., Pawlisch, M.S., Johnston, S.T. & Jackson, M., 2008. Anisotropy of magnetic susceptibility studies in Tertiary ridge-parallel dykes (Iceland), Tertiary margin-normal Aishihik dykes (Yukon), and Proterozoic Kenora-Kabetogama composite dykes (Minnesota and Ontario), *Tectonophysics,* 448**,** 115-124, doi.

Craw, D. & Findlay, R.H., 1985. Hydrothermal alteration of Lower Ordovician granitoids and Devonian Beacon Sandstone at Taylor Glacier, McMurdo Sound, Antarctica, *New Zealand Journal of Geology and Geophysics*, 27**,** 465-475, doi.

deBoer, C.B. & Dekkers, M.J., 1996. Grain-size dependence of the rock magnetic properties for a natural maghemite, *Geophysical Research Letters*, 23**,** 2815-2818, doi.

Dragoni, M., Lanza, R. & Tallarico, A., 1997. Magnetic anisotropy produced by magma flow; theoretical model and experimental data from Ferrar dolerite sills (Antarctica), *Geophysical Journal International*, 128**,** 230-240, doi.

Elliot, D.H. & Fleming, 2008. Physical volcanology and geological relationships of the Jurassic Ferrar Large Igneous Province, Antarctica, *Journal of Volcanology and Geothermal Research* 172**,** 20-37, doi.

Elliot, D.H. & Fleming, T.H., 2000. Weddell triple junction: the principal focus of Ferrar and Karoo magmatism during initial breakup of Gondwana, *Geology*, 28**,** 539-542, doi.

Elliot, D.H., Fleming, T. H., Kyle, P. R., Foland, K. A., 1999. Long-distance transport of magmas in the Jurassic Ferrar Large Igneous Province, Antarctica, *Earth and Planetary Science Letters*, 167**,** 89- 104, doi.

Ernst, R.E. & Baragar, W.R.A., 1992. Evidence from Magnetic Fabric for the Flow Pattern of Magma in the Mackenzie Giant Radiating Dyke Swarm, *Nature*, 356**,** 511-513, doi.

Ernst, R.E. & Buchan, K.L., 1997. Giant radiating dyke swarms: their use in identifying pre-Mesozoic large igneous provinces and mantle plumes. *in Large Igneous Provinces: Continental, Oceanic, and Planetary Volcanism.*, pp. 297-333, ed. Mahoney, J. J., Coffin, M. (Eds.).

Féménias, O., Diot, H., Berza, T., Gauffriau, A. & Demaiffe, D., 2004. Asymmetrical to symmetrical magnetic fabric of dikes: Paleo-flow orientations and Paleo-stresses recorded on feeder-bodies from the Motru Dike Swarm (Romania), *Journal of Structural Geology*, 26**,** 1401-1418, doi.

Ferré, E.C., 2002. Theoretical models of intermediate and inverse AMS fabrics, *Geophysical Research Letters*, 29, doi: 10.1029/2001GL014367.

Fialko, Y.A. & Rubin, A.M., 1999. Thermal and mechanical aspects of magma emplacement in giant dike swarms, *Journal of Geophysical Research-Solid Earth*, 104**,** 23033-23049, doi.

Galland, O., Planke, S., Neumann, E.-R. & Malthe-Sørenssen, A., 2009. Experimental modelling of shallow magma emplacement: Application to saucer-shaped intrusions, *Earth and Planetary Science Letters*, 277**,** 373-383, doi.

Garland, M.J., 2006. Intrusive processes in the Ferrar Province and their role in the evolution of the Geology of Coombs Hills, Antarctica, Bachelor of Science with Honours (Geology), University of Otago, Dunedin.

Guegan, E.B.M., 2006. Shallow intrusion conditions in a flood-basalt province; the story from dykes and a sill offshoot along the contact between a vent complex and country rock; Coombs Hills, Ferrar Province, Antarctica, MSc unpublished MSc Thesis, Otago, Dunedin.

Gunn, B.M. & Warren, G., 1962. Geology of Victoria Land between the Mawson and Mulock Glaciers, Antarctica, *New Zealand Geological Survey Bulletin*, 71**,** 1-157, doi.

Henry, B., 2007. Magnetic Mineralogy, Changes due to heating. *in Encyclopedia of Geomagnetism and Paleomagnetism*, pp. 512-515, eds Gubbins, D. & Herrero-Bervera, E. Springer, Dordrecht, The Netherlands.

Herrero-Bervera, E., Canon-Tapia, E., Walker, G.P.L. & Tanaka, H., 2002. Magnetic fabrics study and inferred flow directions of lavas of the Old Pali Road, O'ahu, Hawaii, *Journal of Volcanology and Geothermal Research*, 118**,** 161-171, doi.

Herrero-Bervera, E., Walker, G.P.L., Cañon-Tapia, E. & Garcia, M.O., 2001. Magnetic fabric and inferred flow direction of dikes, conesheets and sill swarms, Isle of Skye, Scotland, *Journal of Volcanology and Geothermal Research,* 106**,** 195-210, doi.

Isaac, M.J., Chinn, T.J., Edbrooke, S.W. & Forsyth, P.J., 1996. Geology of the Olympus Range area, Southern Victoria Land, AntarcticaInstitute of Geological and Nuclear Sciences, Lower Hutt, N.Z.

Jelinek, V., 1978. Statistical processing of anisotropy of magnetic susceptibility measured on groups of specimen, *Studia Geophyzika et Geodetika,* 22**,** 50-62, doi.

Johnson, A.M. & Pollard, D.D., 1973. Mechanics of growth of some laccolithic intrusions in the Henry mountains, Utah, I: Field observations, Gilbert's model, physical properties and flow of the magma, *Tectonophysics,* 18**,** 261-309, doi.

Kavanagh, J.L., Menand, T. & Sparks, R.S.J., 2006. An experimental investigation of sill formation and propagation in layered elastic media, *Earth and Planetary Science Letters,* 245**,** 799-813, doi.

Knight, M.D. & Walker, G.P.L., 1988. Magma flow directions in dikes of the Koolau complex, Oahu, determined from magnetic fabric studies, *Journal of Geophysical Research,* 93**,** 4301-4319, doi.

Korsch, R.J., 1984. The structure of Shapeless Mountain, Antarctica, and its relation to Jurassic igneous activity, *New Zealand Journal of Geology and Geophysics,* 27**,** 487-504, doi.

Le Maitre, R.W., Batemen, P., Dudek, A., Keller, J., Lameyre Le Bas, M.J., Sabine, P.A., Schmid, R., Sorensen, H., Streckeisen, A., Wolley, A.R. & Zanettin, B., 1989. *A classification of igneous rocks and glossary terms,* edn, Vol., pp. Pages, Blackwell, Oxford.

Leat, P.T., 2008. On the long-distance transport of Ferrar magmas. *in Structure and emplacement of high-level magmatic systems,* pp. 45-61Geological Society, London, Special Publications.

Lowrie, W., 1990. Identification of ferromagnetic minerals in a rock by coercivity and unblocking temperature properties, *Geophysical Research Letters,* 17**,** 159-162, doi.

Lowrie, W., 1997. Fundamentals of geophysics, pp. 354 pp.Cambridge University Press.

Maccaferri, F., Bonafede, M. & Rivalta, E., 2011. A quantitative study of the mechanisms governing dike propagation, dike arrest and sill formation, *Journal of Volcanology and Geothermal Research,* 208**,** 39-50, doi: 10.1016/j.jvolgeores.2011.09.001.

Menand, T., 2009. Physical controls and depth of emplacement of igneous bodies: A review, *Tectonophysics,* doi: 10.1016/j.tecto.2009.10.016.

Mudge, M.R., 1968. Depth control of some concordant intrusions., *Geological Society of America Bulletin,* 79**,** 315–332, doi.

Muirhead, J.D., Airoldi, G., Rowland, J.V. & White, J.D.L., 2011. Interconnected sills and inclined sheet intrusions control shallow magma transport in the Ferrar large igneous province, Antarctica, *Geological Society of America Bulletin,* doi: 10.1130/b30455.1.

Norrish, K. & Chappell, B.W., 1977. X-ray fluorescence spectrometry. *in Physical Methods of Determinative Mineralogy, 2nd Edition.,* pp. 201-272, ed. Zussman, J. Academic Press, London.

Pollard, D.D., Muller, O.H. & Dockstader, D.R., 1975. The form and growth of fingered sheet intrusions, *Geological Society of America Bulletin,* 86**,** 351-363, doi.

Polteau, S., Mazzini, A., Galland, O., Planke, S. & Malthe-Sørenssen, A., 2008. Saucer-shaped intrusions: Occurrences, emplacement and implications, *Earth and Planetary Science Letters,* 266**,** 195-204, doi.

Potter, D.K., 2004. A comparison of anisotropy of magnetic remanence methods -- a user's guide for application to palaeomagnetism and magnetic fabric studies, *Geological Society, London, Special Publications,* 238**,** 21-35, doi: 10.1144/gsl.sp.2004.238.01.03.

Potter, D.K. & Stephenson, A., 1988. The Importance of Remanence Anisotropy in Magnetic Fabric Analysis and in Paleomagnetism, *Geophysical Journal-Oxford,* 92**,** 548-548, doi.

Raposo, M.I.B. & Ernesto, M., 1995. Anisotropy of magnetic susceptibility in the Ponta Grossa dike swarm (Brazil) and its relationship with magma flow directions, *Physics of the Earth and Planetary Interiors,* 102**,** 183-196, doi.

Rochette, P., Aubourg, C. & Perrin, M., 1999. Is this magnetic fabric normal? A review and case studies in volcanic formations, *Tectonophysics,* 307**,** 219-234, doi.

Rollinson, H., 1993. *Using geochemical data: Evaluation, presentation, interpretation,* edn, Vol., pp. Pages, Longman Scientific & Technical, Essex, England.

Ross, P.-S., White, J.D.L. & McClintock, M., 2008. Geological evolution of the Coombs-Allan Hills area, Ferrar Large Igneous Province, Antarctica: debris avalanches, mafic pyroclastic density currents, phreatocauldrons., *Journal of Volcanology and Geothermal Research,* 172**,** 38-60, doi.

Tarling, D.H. & Hrouda, F., 1993. The magnetic anisotropy of rocks, pp. 217Chapman and Hall, London.

Tauxe, L., Gee, J.S. & Staudigel, H., 1998. Flow directions in dikes from anisotropy of magnetic susceptibility data: the bootstrap way, *Journal of Geophysical Research,* 103**,** 17775-17790, doi.

Thomson, K., 2007. Determining magma flow in sills, dykes and laccoliths and their implications for sill emplacement mechanisms., *Bulletin of Volcanology,* doi: 10.1007/s00445-007-0131-8.

Weinberger, R., Lyakhovsky, V., Baer, G. & Agnon, A., 2000. Damage zones around en echelon dike segments in porous sandstone, *Journal of Geophysical Research,* 105**,** 3115-3133, doi.

White, J.D.L., Bryan, S.E., Ross, P.-S., Self, S. & Thordarson, T., 2009. Physical volcanology of Large Igneous Provinces: update and review. *in The Legacy of George Walker*, pp. 291-321Special Publications of IAVCEI, London.

White, J.D.L. & Garland, M.J., 2007. Shoaling sills of a Large Igneous Province: sills and dikes at Coombs Hills, Ferrar Province, Antarctica. *in EGU 2007*.

Winchester, J.A. & Floyd, P.A., 1977. Geochemical discrimination of different magma series and their differentiation products using immobile elements, *Chemical Geology,* 20**,** 325-343, doi.

Winter, 2001. An introduction to igneous and metamorphic petrology, pp. 697Prentice Hall, Upper Saddle River, NJ, United States (USA).

Figure captions

Fig. 1 – Location map and regional geology along the Transantarctic Mountains (TAM). Sketch of Ferrar Dolerite distribution, redrawn from Muirhead *et al*. (2011); boxed area localizes the Allan-Coombs Hills region, also represented on the right. CTM= Central Transantarctic Mountains; DV= Dry Valleys; SVL, NVL= South and North Victoria Land.

Fig. 2 – Left – Map of Allan Hills most intruded region. Numbers refer to diabase *sheets* sampled for petro-physical analysis. Stereoplots show the average of macroscopic lineations (see text for further explanation). Right – **a**. sketch of sheet segments: I - curved offset and overlapping segment tips; II – 'horns'; III – 'steps'. **b-c**. Kinematic indicators along the margins of #03.

Fig. 3 – Photomicrographs of Allan Hills A_I [**a-b**] and A_{II} dolerites [**c-d**]. Details of sample OU 78929, with a glomeroporphyritic texture: **a**. large clinopyroxene phenocryst immersed in (black) groundmass of both crystals and glass (polarized light); **b**. plagioclase with 'hopper' texture and dark groundmass (plane light). **c**. Radiating plagioclase blades in the groundmass of OU 78995, plane light; **d**. Plagioclase crystals immersed in glass in section of OU 78999, plane light**.**

Fig. 4 – a. Representative bivariate diagrams of major and trace elements (see Table 1). **b**. Igneous rock classification diagrams; left – TAS classification after Le Maitre et al. (1989), right – Winchester and Floyd (1977). Major element data normalized to 100% on a volatile-free basis.

Fig. 5 – Histogram of the mean susceptibility (K_m) distribution for the 84 analyzed Ferrar Dolerite samples. For ease of visualization only part of the sample codes is represented. The inset histogram [a] shows the percentage of 'low'-, 'intermediate' and 'high-susceptibility' specimens for sheet sets A_I and A_{II} (in SI).

Fig. 6 – Thermomagnetic behaviour of **a**. 'low-', **b**. 'intermediate-' and **c**. 'high-susceptibility' specimens (see text). Each row of diagrams corresponds to temperature-dependent susceptibility, progressive demagnetization of three-component IRM and isothermal remanent magnetization acquisition and demagnetization measurements, from top to bottom.

Fig. 7 – Relationship between magnetic fabric data and igneous intrusions. Left – Simplified sketch of #04-7 and enlarged detail of one of its segments (section #05, see Table 3.a). Top right – Theoretical model of imbrication of crystals along sheet's walls; MFP= magnetic foliation plane; DPL= dyke plane. Bottom right – Stereoplot of AMS and AIRM data, sections #05A/B; N= normal fabric.

Fig. 8 – Fabric types within Allan Hills AMS and AIRM dataset. Left –Site 78976: (**a**) inverse (R) AMS fabric (**b**) normal AIRM fabric. Data are superimposed on the rose diagram of sheet #11's strike. **c**. P_J-T diagram highlighting variable ellipticity of magnetic fabric within AMS and AIRM data. **d**. Linear relationship among the normalized values of the axes of magnetic susceptibility and magnetic remanence anisotropy ellipsoids. Right – Examples of intermediate fabric (see text).

Fig. 9 – Interpretation of Allan Hills sheet intrusions upon magnetically inferred flow directions. Left – Magma infilled A_I cracks by predominantly lateral flow (flow plunge <45°). Right – segmented A_{II} inclined sheets converge towards a common area of intersection (source?), but magma flow, as recorded by their rock magnetic fabric, varied greatly with intrusion geometry.

Fig. 10 – Magma flow-fabric from small segments (AMS from their cores at the top left of the figure) and their tips (AMS and AIRM, bottom right). See Table 2.a and text.

Figures

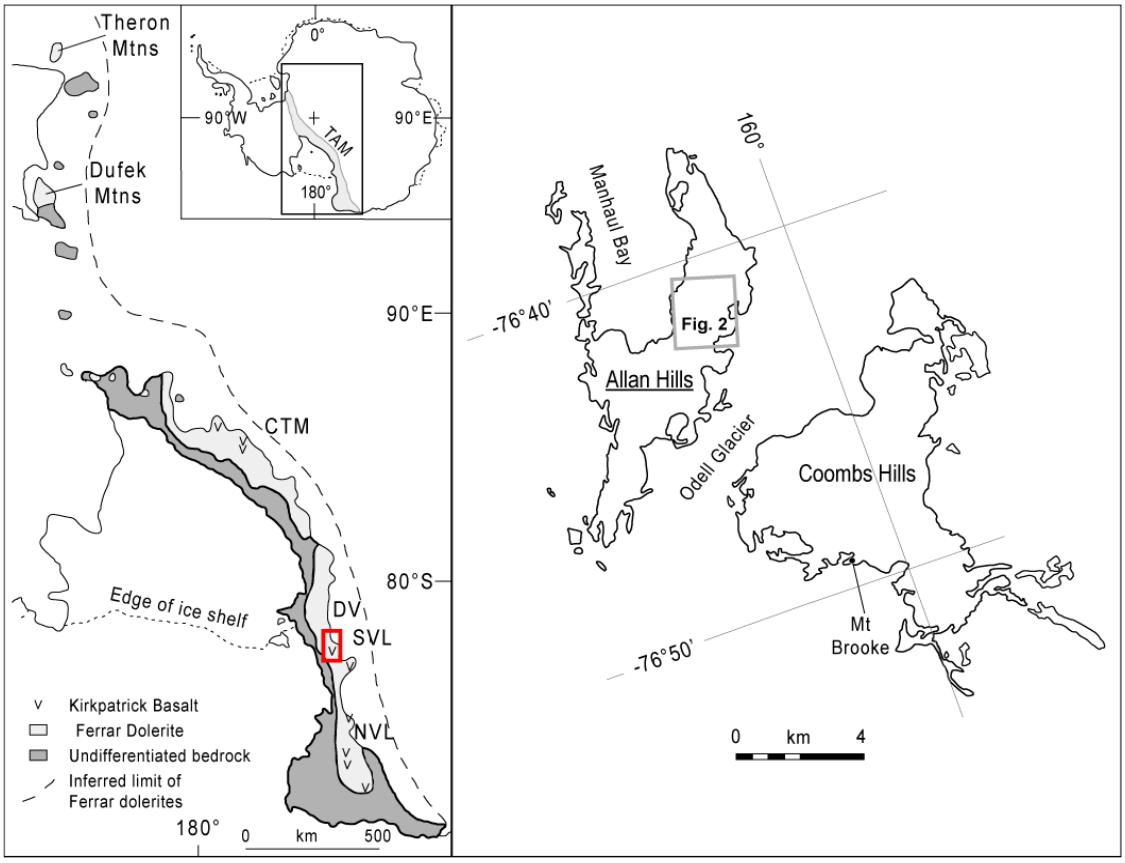

Fig. 1

Fig. 2

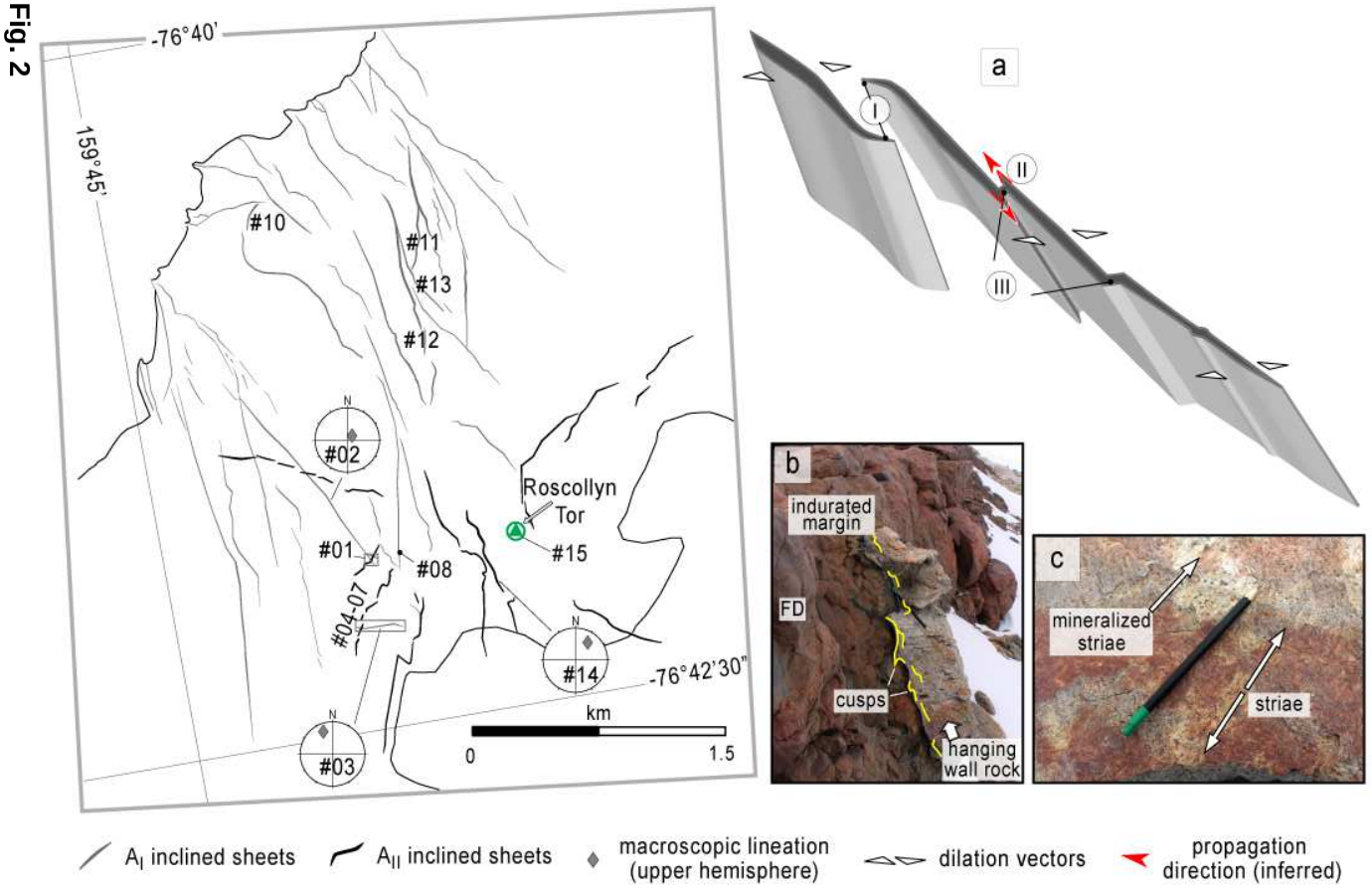
-76°40'
159°45'
#10
#11
#13
#12
#02
Roscollyn
Tor
#15
#01
#08
#04-07
#14
-76°42'30"
#03
km
0
1.5
a
I
II
III
b
indurated
margin
FD
cusps
hanging
wall rock
c
mineralized
striae
striae
A_I inclined sheets
A_II inclined sheets
macroscopic lineation
(upper hemisphere)
dilation vectors
propagation
direction (inferred)

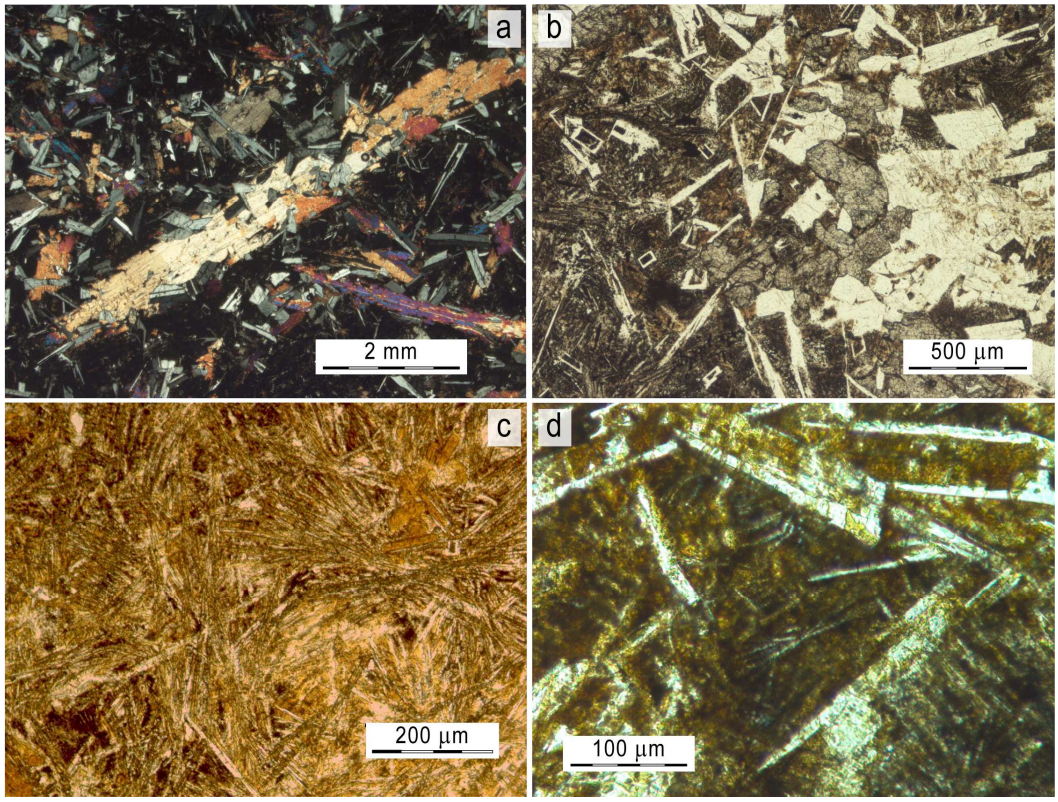

Fig. 3

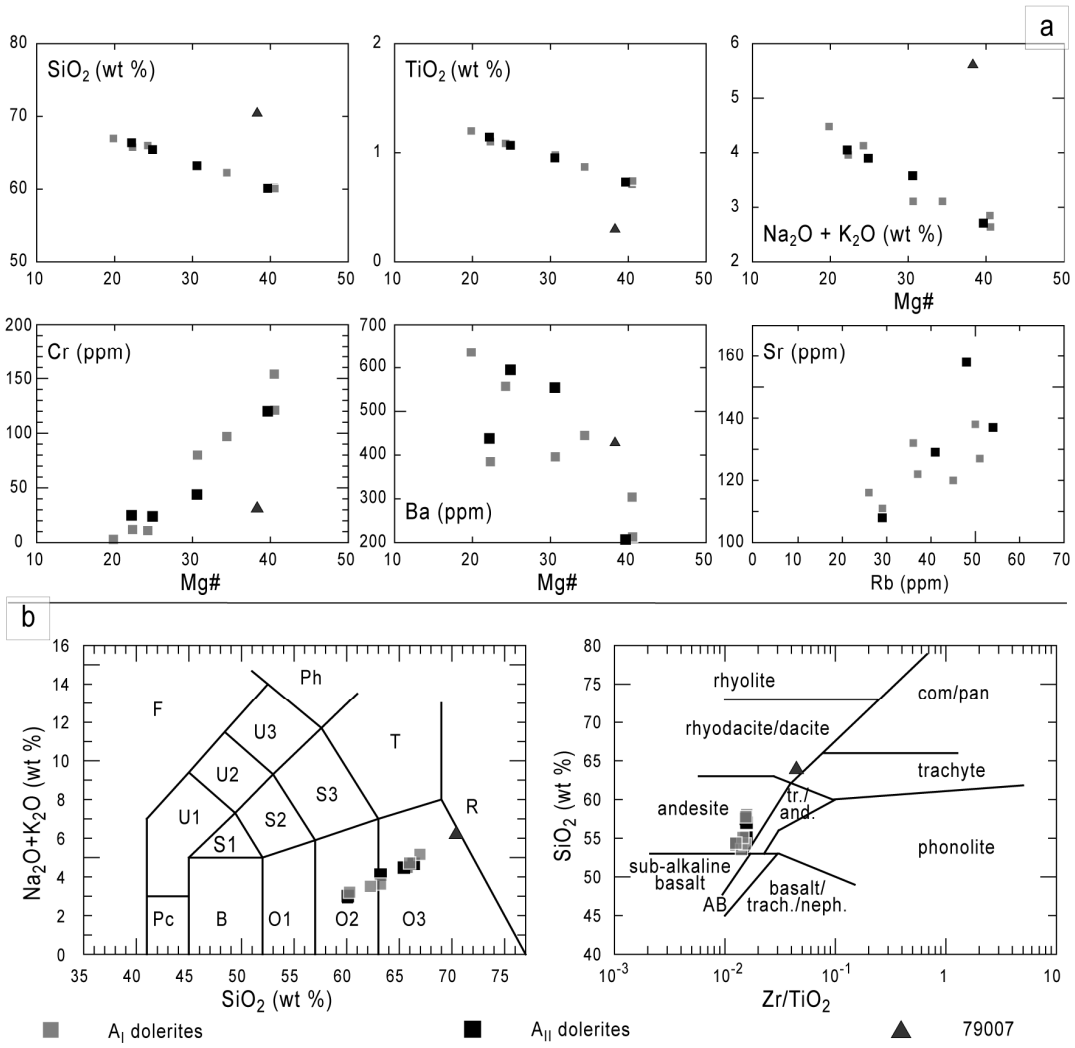
a
SiO2 (wt %)
TiO2 (wt %)
Na2O + K2O (wt %)
Mg#
Cr (ppm)
Mg#
Ba (ppm)
Mg#
Sr (ppm)
Rb (ppm)
b
Na2O+K2O (wt %)
SiO2 (wt %)
F
Ph
U3
T
U2
S3
U1
S2
R
S1
Pc
B
O1
O2
O3
SiO2 (wt %)
rhyolite
com/pan
rhyodacite/dacite
trachyte
andesite
tr./
and.
phonolite
sub-alkaline
basalt
AB
basalt/
trach./neph.
Zr/TiO2
AI dolerites
AII dolerites
79007

Fig. 4

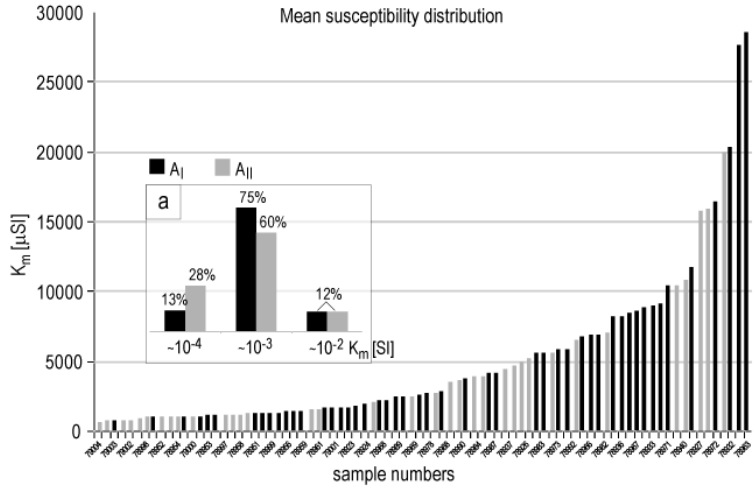
Mean susceptibility distribution
K_m [µSI]
sample numbers
A_I
A_{II}
a
13%
28%
75%
60%
12%
~10-4
~10-3
~10-2 K_m [SI]

Fig. 5

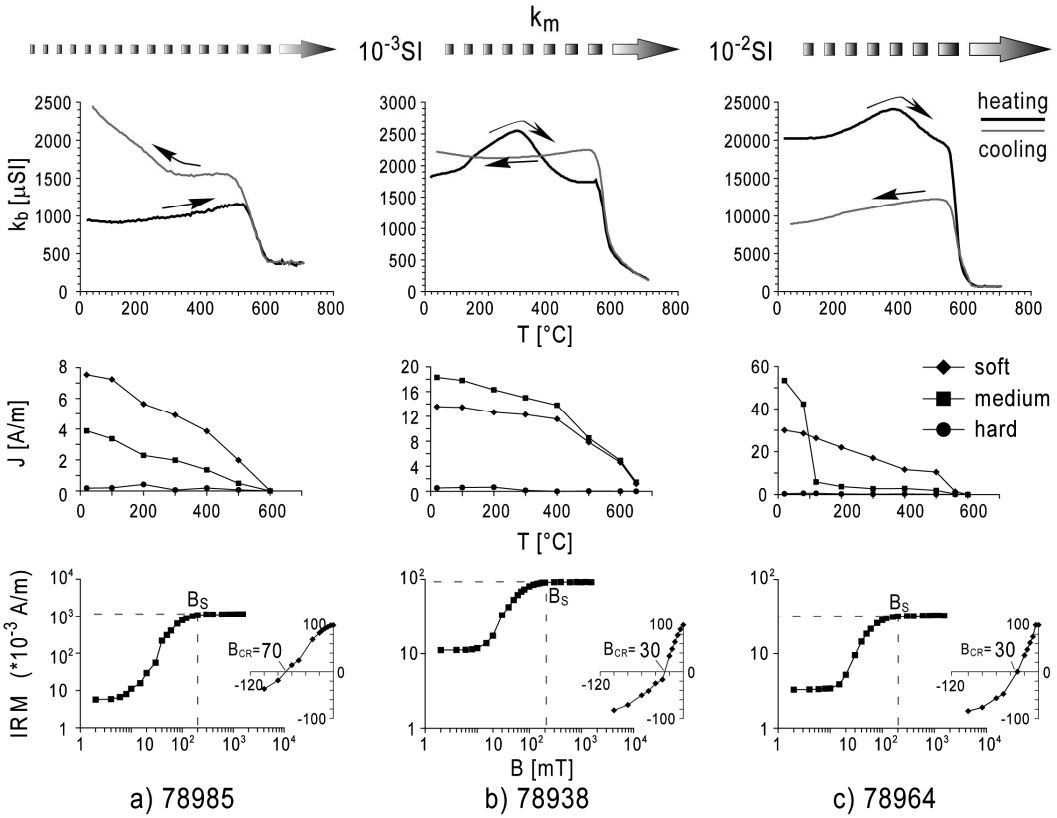
k_m
10-3SI
10-2SI
k_b [µSI]
T [°C]
heating
cooling
J [A/m]
soft
medium
hard
IRM (*10-3 A/m)
Bs
BCR=70
BCR= 30
B [mT]
a) 78985
b) 78938
c) 78964

Fig. 6

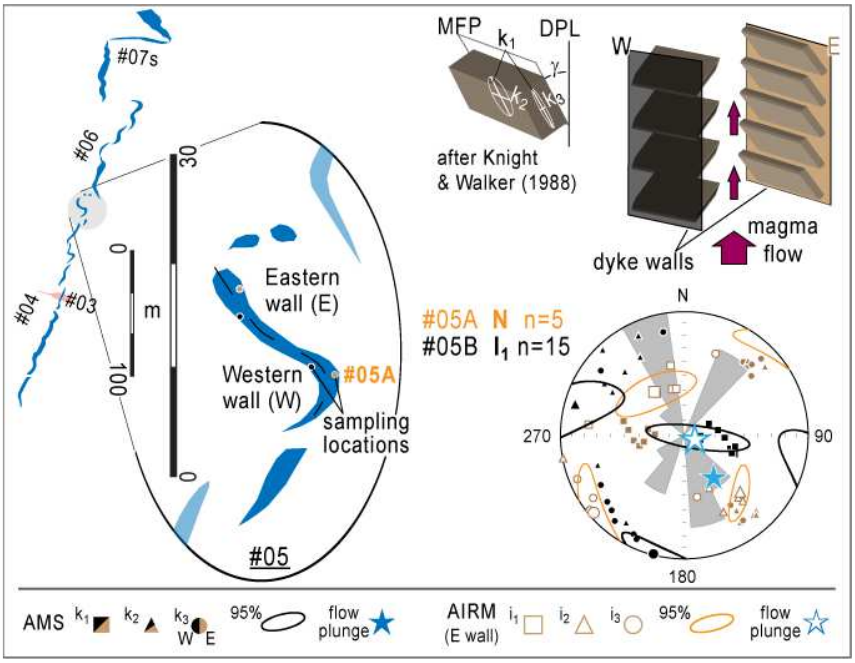
#07s
#06
#04
#03
30
0
m
100
0
Eastern
wall (E)
Western
wall (W)
#05A
sampling
locations
#05
MFP
k1
DPL
γ
k2
k3
after Knight
& Walker (1988)
W
E
magma
flow
dyke walls
#05A N n=5
#05B I1 n=15
N
270
90
180
AMS k1 k2 k3 W E 95% flow plunge
AIRM (E wall) i1 i2 i3 95% flow plunge

Fig. 7

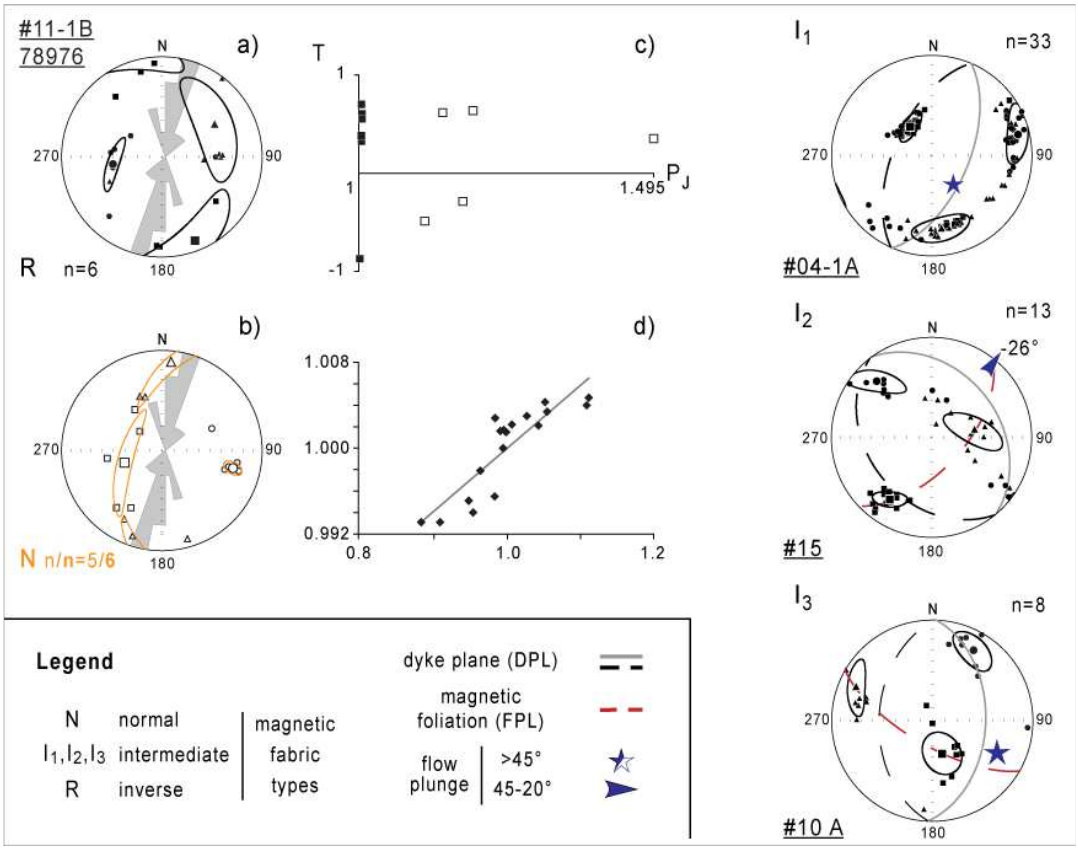
#11-1B
78976
a)
N
270
90
180
R n=6
T
1
1
-1
c)
1.495
P_J
b)
N n/n=5/6
1.008
1.000
0.992
0.8
1.0
1.2
d)
I_1
n=33
#04-1A
I_2
n=13
26°
#15
I_3
n=8
#10 A
Legend
N normal
I_1, I_2, I_3 intermediate
R inverse
magnetic fabric types
dyke plane (DPL)
magnetic foliation (FPL)
flow plunge
>45°
45-20°

Fig. 8

Fig. 9

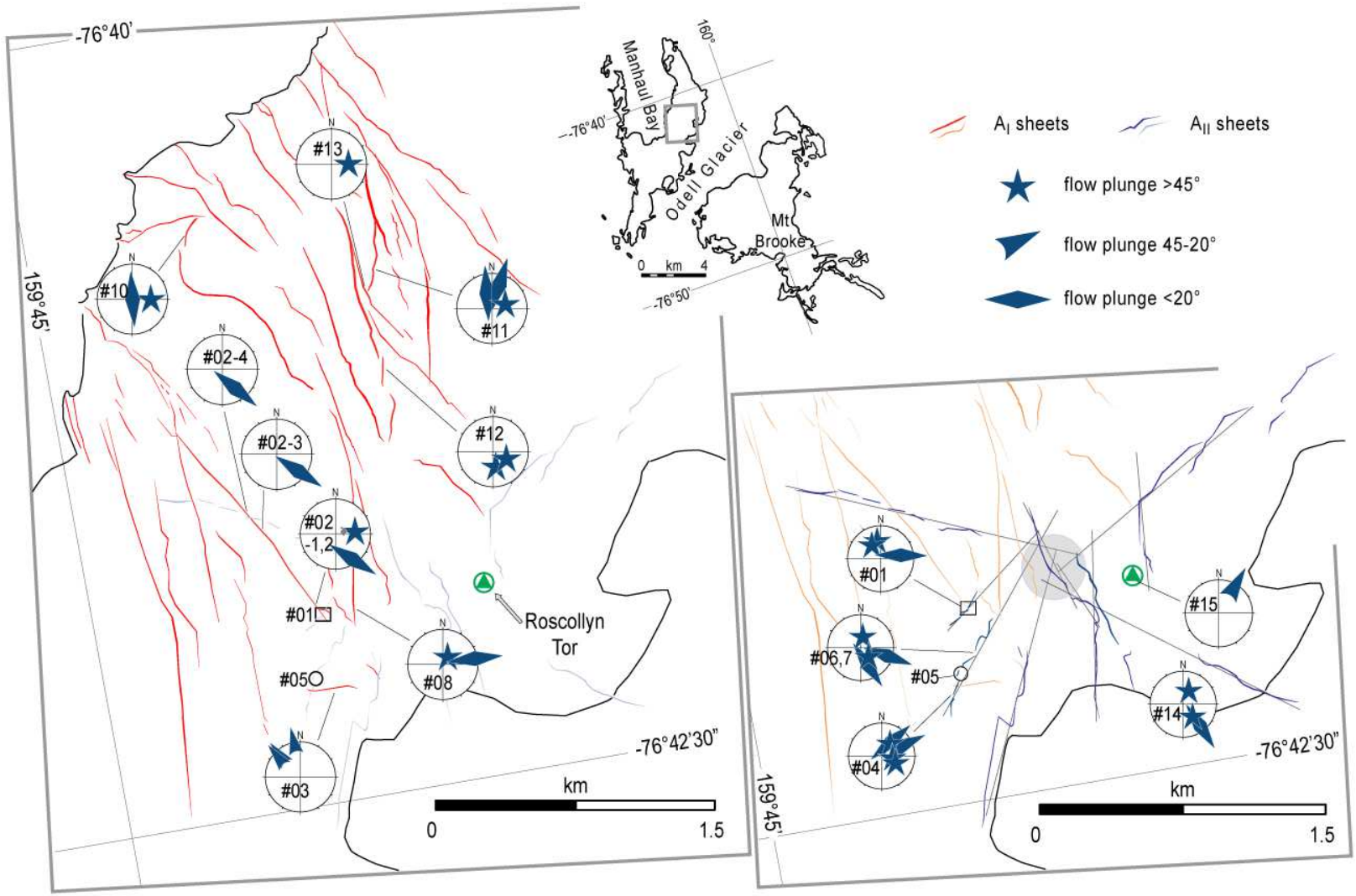
-76°40'
159°45'
#13
#10
#11
#02-4
#02-3
#12
#02
-1,2
#01
#05
#08
#03
Roscollyn
Tor
-76°42'30"
km
0
1.5
Manhaul Bay
Odell Glacier
Mt
Brooke
160°
-76°40'
-76°50'
0 km 4
AI sheets
AII sheets
flow plunge >45°
flow plunge 45-20°
flow plunge <20°
#01
#06,7
#05
#04
#15
#14
-76°42'30"
159°45'
km
0
1.5

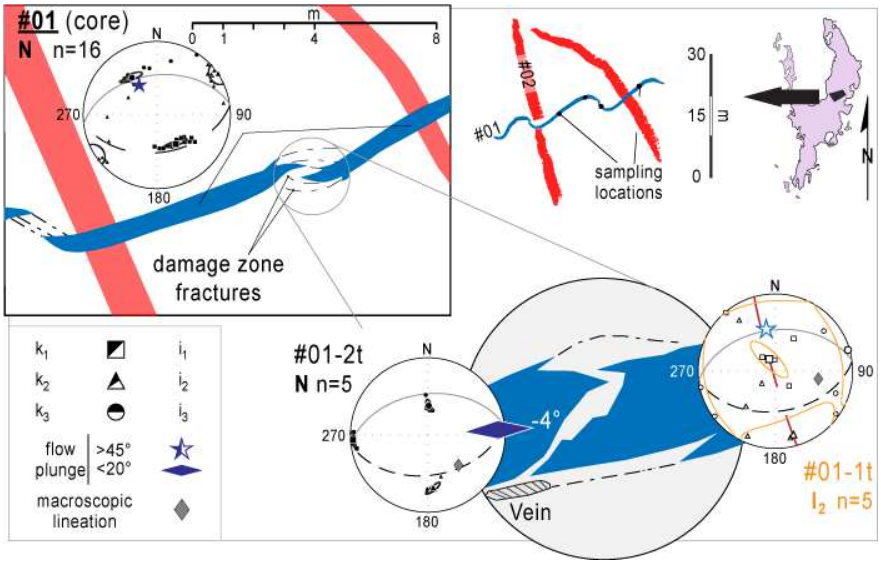
#01 (core)
N n=16
m
0 1 4 8
N
270
90
180
damage zone
fractures
#02
#01
sampling
locations
30
15
0
N
k1 i1
k2 i2
k3 i3
flow >45°
plunge <20°
macroscopic
lineation
#01-2t
N n=5
N
270
180
-4°
Vein
N
270
90
180
#01-1t
I2 n=5

Fig. 10

Tables

	A_I inclined sheets							A_{II} inclined sheets			
dyke	#02	#03	#08	#10	#11	#12	#13	#01	#04	#05	#14
sample	78928	78938	78964	78968	78975	78985	78993	78923	78943	78954	78996
SiO_2	60.28	63.22	65.75	66.96	62.25	65.99	60.08	66.38	63.22	60.10	65.43
TiO_2	0.71	0.98	1.10	1.20	0.87	1.09	0.74	1.14	0.95	0.73	1.07
Al_2O_3	16.45	16.40	15.34	15.52	16.30	15.50	16.58	15.44	17.15	16.43	16.28
$Fe_2O_3^T$	9.95	11.28	11.81	12.32	10.68	11.62	9.95	12.04	11.49	10.12	11.69
MnO	0.20	0.22	0.20	0.20	0.21	0.19	0.20	0.23	0.24	0.20	0.20
MgO	7.62	5.80	3.85	3.52	6.33	4.25	7.50	3.96	5.81	7.37	4.44
CaO	11.42	9.60	9.09	7.25	10.38	8.10	11.88	7.99	8.37	12.07	7.93
Na_2O	2.14	2.30	2.85	3.18	2.17	2.91	2.02	2.68	2.27	2.11	2.82
K_2O	1.07	1.33	1.65	1.98	1.34	1.80	0.90	2.00	1.84	0.90	1.65
P_2O_5	0.10	0.15	0.17	0.20	0.14	0.17	0.10	0.18	0.15	0.10	0.17
LOI	60.28	63.22	65.75	66.96	62.25	65.99	60.08	66.38	63.22	60.10	65.43
Tot. %	99.47	98.98	100.25	100.62	99.84	100.19	100.59	100.56	100.55	100.48	100.37
Mg#	40.49	30.63	22.30	19.84	34.40	24.25	40.56	22.17	30.57	39.65	24.87
Sc	39	45	41	42	42	41	39	44	47	37	46
V	233	262	253	267	244	250	224	257	294	227	280
Cr	154	80	12	3	97	11	121	25	44	120	24
Ni	75	49	32	25	56	28	75	26	46	75	36
Cu	83	103	129	137	95	117	91	119	100	99	114
Zn	80	94	99	107	89	100	78	102	97	78	101
Ga	15	17	17	18	15	16	15	16	17	15	18
As	b.d.l.	2	3	1	1	2	1	1	2	b.d.l.	1
Rb	26	36	45	50	37	51	29	54	48	29	41
Sr	116	132	120	138	122	127	111	137	158	108	129
Y	23	31	35	38	28	34	23	35	30	23	34
Zr	89	128	153	164	112	147	84	153	130	84	146
Nb	3	3	4	7	2	5	2	6	4	b.d.l.	5
Ba	304	396	385	636	445	557	213	438	554	207	595
La	14	21	26	33	19	35	18	26	18	7	22
Ce	33	39	57	49	39	50	31	46	37	30	48
Nd	16	22	31	27	16	23	15	28	19	16	21
Pb	8	9	10	13	10	10	7	11	9	8	11
Th	3	4	5	5	5	5	3	5	5	3	5
U	3	4	4	2	1	2	1	2	3	1	2

Table 1 – Normalized major element (wt % oxides) and trace element (ppm) concentrations were determined by a Phillips PW 2400 XRF spectrometer unit (operator D. Walls, procedure after Norrish and Chappell, 1977). LOI = loss on ignition. 'b.d.l.'= below detection limit. Mg# is the ratio MgO*100/(MgO+FeO^T). $Fe_2O_3^T$ was converted to FeO^T using a 0.9 conversion factor.

ALLAN HILLS																
Section / Segment	dyke trend*	n/N	k_1		95% conf. angles	k_2		95% conf. angles	k_3		95% conf. angles	Angle k_1** with DPL	Angle FPL with DPL	Fabric type	Flow direction from magnetic fabric ***	Macroscopic lineation ***
			D	I		D	I		D	I						
#01-1t	081/55° S	5/5	331	76	26.5 / 8.2	165	14	42.9 / 23.0	74	3	43.3 / 11.6	42°		O, I_2	348 / -55°	horns: 100/-43°
#01		16/16	147	51	12.4 / 2.5	57	0	13.4 / 8.8	326	39	10.9 / 3.7	1°	20°	P, N	327 / -51°	
#01-2t		5/5	266	4	6.8 / 2.5	174	31	9.1 / 2.4	2	59	6.8 / 2.5	6°	25° imbr.	P, N	086 / -04°	horn: 134/-44°
#02-1	138/48° SW	7/7	303	16	11.2 / 2.1	196	46	22.8 / 4.7	47	40	23.3 / 7.7	0°	2° imbr.	P, N	123 / -16°	
#02-2		6/6	276	56	7.5 / 3.0	53	26	7.9 / 3.2	154	20	4.2 / 2.6	16°		O, I_2	083 / -42°	striae: 065/-30°
#02-3		5/5	303	71	8.1 / 7.9	117	19	32.7 / 7.8	208	2	32.7 / 7.8	35°		P, I_1	119 / -19°	
#02-4		10/10	284	7	20.4 / 8.3	15	13	20.3 / 10.0	166	75	10.9 / 7.4	19°		O, I_1	127 / -12°	
#03-1	089/31° S	6/6	189	66	3.6 / 2.3	299	9	14.5 / 2.5	33	22	14.6 / 3.2	23°		P, I_1	312 / -22°	average of striae: 339/-25°
#03-2		30/34	315	1	12.4 / 7.5	225	31	46.7 / 8.1	47	59	46.8 / 6.9	8° (k_2)	24°	P, N	010 / -27°	
#03-3		25/36	130	48	21.6 / 10.1	340	38	29.6 / 13.9	238	15	30.7 / 14.3	24°		O, I_2	322 / -22°	
#04-1A	193/60° W	25/28	322	59	8.6 / 2.9	178	26	19.6 / 6.2	80	16	19.6 / 6.7	5°		P, I_1	142 / -59°	adjoined segments: lateral crack-tip propagation
#04-1B		6/7	245	33	36.2 / 7.9	141	21	35.6 / 14.0	25	50	15.2 / 12.3	17°		P, I_2	065 / -33°	
#04-2		11/12	220	59	9.0 / 1.3	321	7	9.2 / 6.1	55	30	6.8 / 2.6	13°		P, I_1	040 / -59°	
#04-3		5/6	286	63	48.9 / 20.4	126	26	55.7 / 26.7	32	8	52.2 / 4.3	3°		O, I_2	106 / -63°	
#04-4t		6/8	113	78	14.3 / 6.7	224	4	9.7 / 1.6	314	11	14.9 / 3.8	24° (k_2)	39° imbr.	O, I_3	NE-SW lineation (N216°)	
#05A	153° W	5/5	325	55	27.5 / 10.9	137	35	18.5 / 5.6	229	4	27.8 / 8.4	1°	17°	O, N	145 / -55°	
#05B		15/22	100	81	34.8 / 7.5	285	9	36.1 / 12.5	195	1	18.5 / 7.9	12°		P, I_1(s)	113 / -83°	
#06-1t	# 160/60° W	11/11	66	77	7.0 / 4.1	328	2	7.1 / 4.3	237	12	8.0 / 3.9	9° (k_2)	44° imbr.	O, I_3	NW-SE lineation (N150°)	# local tip orientation

Table 2a (previous page) **–** AMS/AIRM fabric and average and/or local orientation of dolerite intrusions at Allan Hills. n/N= number of specimens; D= declination; I= inclination; D and I coordinates are given for the upper hemisphere of a reference stereographic projection. (*) Strike, dip, dip direction; (**) proximity/angle between k_2 (or i_2) and the dyke plane (characterizes nearly normal, oblate I_3 fabric types); (***) trend, plunge, upper hemisphere; (s)='scissored' fabrics; 'imbr.'=angle of imbrication and not simply the angle formed by intersection between magnetic foliation and dyke plane (normal and I_3 fabric types); #=local strike of the dyke parallel to the orientation of a macroscopic kinematic indicator.

Table 2b (next page) – Continued from previous.

ALLAN HILLS (continued)

Section / Segment	dyke trend*	n/N	k_1 D	k_1 I	95% conf. angles	k_2 D	k_2 I	95% conf. angles	k_3 D	k_3 I	95% conf. angles	Angle k_1** with DPL	Angle FPL with DPL	Fabric type	Flow direction from magnetic fabric ***	Macroscopic lineation ***
#06-2	201/58° W	15/16	190	61	31.0 / 6.7	58	20	34.7 / 7.6	320	20	36.0 / 6.9	33°		P, I_1(s)	010 / -61°	
#06-3		13/13	296	51	23.8 / 8.3	110	38	27.8 / 10.4	202	3	20.0 / 6.6	7°		P, I_2(s)	116 / -51°	striae: 119/-58°
#07s	255/20° N	9/9	107	3	5.3 / 1.9	9	70	9.2 / 3.5	198	19	9.0 / 3.4	13°		P, I_1	112 / -12°	
#08-1	082/72° S	12/15	259	11	22.9 / 13.3	15	67	72.7 / 15.5	165	21	72.8 / 10.9	1°		P, I_1	079 / -11°	ramp-structure: inclined upward flow towards the E
#08-2		6/7	162	28	4.0 / 0.0	304	56	5.6 / 0.0	62	18	5.5 / 1.9	43°		P, I_2	027 / -69°	
#10	182/46° W	8/14	164	62	18.5 / 14.4	293	19	20.6 / 8.0	30	20	17.4 / 11.7	24° (k_2)	34°	O, I_3	099 / -45°	
#10-t		5/5	184	64	12.6 / 2.6	356	26	11.4 / 3.9	88	3	7.3 / 4.3	14° (i_2)	41°	O, I_3	N-S lineation (N178°)	
#11-1A	190/39° W	11/17	173	1	14.8 / 3.1	74	82	14.6 / 4.4	263	8	5.1 / 4.1	11°		O, I_2	N-S lineation (N173°)	
#11-1B		5/6	252	58	45.1 / 6.1	6	15	45.0 / 5.1	104	28	9.4 / 4.0	9° (i_2)	23°	O, I_3	N-S lineation (N017°)	
#11-2		6/11	229	62	12.6 / 1.1	352	16	17.3 / 11.7	89	23	16.9 / 2.8	30°	29° imbr.	P, N	049 / -62°	
#12-2	186/39° W	14/16	298	57	16.5 / 5.5	55	17	16.9 / 6.4	154	28	19.5 / 11.9	20°		P, I_1(s)	118 / -57°	
#12-3		8/9	350	54	6.1 / 4.1	199	33	21.1 / 4.3	100	14	20.7 / 3.7	32°	37°	P, N	170 / -54°	
#13	129/70°S	12/17	270	50	25.5 / 5.3	175	5	48.0 / 11.0	81	40	45.8 / 5.7	7°		P, I_1	090 / -50°	
#14-1	152/58° SW	7/8	307	13	22.2 / 1.6	38	5	36.4 / 20.4	148	76	36.2 / 17.4	13°		P, I_1	143 / -14°	striae: 045/-36°
#14-2A		10/18	260	32	21.4 / 7.4	142	38	16.6 / 7.3	17	36	17.3 / 7.3	24°	37°	O, N	029 / -54°	horn: 015/-48°
#14-2B		7/7	322	52	33.0 / 7.1	138	38	42.1 / 30.8	229	2	41.3 / 10.4	19°	36°	P, N	142 / -52°	
#15	142/30° SW	11/12	214	26	9.1 / 6.1	81	54	23.6 / 8.9	316	23	23.6 / 6.2	3°		P, I_2	034 / -26°	striae: 035/-34°